IOP Publishing Superconductor Science and Technology
Supercond. Sci. Technol. 31 (2018) 034006 (6pp) https://doi.org/10.1088/1361-6668/aaa858

Effects of heavy-ion irradiation on the microwave surface impedance of $(Ba_{1-x}K_x)Fe_2As_2$ single crystals

G Ghigo[1,2,4], D Torsello[1,2], R Gerbaldo[1,2], L Gozzelino[1,2,4], F Laviano[1,2] and T Tamegai[3]

[1] Politecnico di Torino, Department of Applied Science and Technology, Torino, Italy
[2] Istituto Nazionale di Fisica Nucleare, Sez. Torino, Italy
[3] The University of Tokyo, Department of Applied Physics, Tokyo, Japan

E-mail: gianluca.ghigo@polito.it and laura.gozzelino@polito.it

Received 31 October 2017, revised 4 January 2018
Accepted for publication 17 January 2018
Published 14 February 2018

Abstract

The electrodynamic response of $Ba_{1-x}K_xFe_2As_2$ single crystals at the microwave frequencies has been investigated by means of a coplanar resonator technique, at different values of non-magnetic disorder introduced into the samples by heavy-ion irradiation. The surface impedance $Z_s = R_s + iX_s$ conforms to the classical skin effect above the critical temperature. Below T_c, R_s monotonically decreases while X_s shows a peak, which evolves as a function of the irradiation fluence. The disorder-dependent $Z_s(T)$ curves are analyzed within a two-fluid model, suitably modified to account for a finite quasiparticle fraction at $T = 0$. The analysis gives, for the unirradiated crystal, quasiparticle relaxation times τ that are in good agreement with previous literature. Smaller τ values are deduced for the disordered crystals, both in the normal and in the superconducting states. The limits of application of the model are discussed.

Keywords: iron-based superconductors, heavy-ion irradiation, microwave surface impedance

(Some figures may appear in colour only in the online journal)

1. Introduction

The iron-based superconductors (IBS), and the $BaFe_2As_2$-based compounds in particular, are nowadays among the most studied examples of unconventional superconductivity. A comprehensive understanding of their properties should also cover the treatment of disorder effects in an appropriate way. To this aim, particle irradiation is a particularly valuable tool, because it is the way to induce controlled defects into the material without contributing extra charge or significant structural distortion, contrary to most cases of chemical substitutions. Several irradiation experiments have been performed in the last years, with a large variety of particle beams and compounds [1–18], but an ultimate picture of the role of disorder in IBS has not been reached yet. The debate on this topic is still open, and deserves further experimental and theoretical investigations. Particle irradiation techniques are of great interest also because, beside the study of fundamental properties of IBS, they are relevant to the investigation of the application potential. In fact, in addition to robustness to impurities for what concerns the critical temperature, proving the ability of manipulating their basic properties by suitable disorder would make IBS appealing in a number of device applications.

In this work, we present an experimental approach to investigate the microwave properties of $Ba_{1-x}K_xFe_2As_2$ single crystals, in samples where disorder is progressively increased by means of 250 MeV Au-ion irradiation. The same samples were recently investigated [11] in terms of disorder-induced modifications of penetration depth. It was shown that the huge increase of λ_L in spite of a small decrease of T_c can be explained within the $s\pm$ wave model, when at least three bands are considered. Nevertheless, the discussion about the fundamental mechanisms of superconductivity in IBS is still

[4] Authors to whom any correspondence should be addressed.

open, and some results are not only consistent with the $s\pm$ model, but could also be explained within a conventional multiband model. The issue deserves further investigations, though it is beyond the scope of this work. Here we focus on the electrodynamic response, represented by the complex surface impedance. A phenomenological modified two-fluid analysis is proposed, leading to a satisfactory agreement with literature for what concerns the pristine compound and giving a hint on the effects of ion irradiation on the electrodynamic parameters such as the quasiparticle relaxation time. The microwave characterization technique is a novel cavity-perturbation approach, involving the use of superconducting coplanar resonators.

2. Techniques

2.1. Sample preparation

High-quality $Ba_{1-x}K_xFe_2As_2$ (K-Ba122) crystals with an analyzed doping level of $x = 0.42$ and a critical temperature $T_c \approx 38$ K were grown by the FeAs self-flux method [7]. All the investigated crystals were cleaved to be thin plates with thickness of about 10 μm, more than ten times smaller than the width and length.

2.2. Microwave characterization

In order to study its microwave properties, the K-Ba122 crystal under study was coupled to a coplanar waveguide resonator. The resonator was patterned on a 250 nm thick $YBa_2Cu_3O_{7-x}$ (YBCO) film with a critical temperature of about 88 K, grown on an MgO substrate [19]. The resonance curves were measured in a Cryomech PT 415 pulse tube cooler by means of a Rohde Schwarz ZVK vector network analyzer. An input power of −40 dBm, well below the non-linearity threshold of the resonator [20], was used. Coplanar resonators were previously used to study the microwave response of cuprate superconductors and magnesium diboride, as well as the effects of heavy-ion irradiation on their properties [21–24]. Here, the measurement of the K-Ba122 crystals is based on the exploitation of a region where the YBCO-resonator rf fields are uniform enough, i.e. far from the stripline edges. Figure 1(a) shows two examples of resonance curves (S_{21} is the transmission coefficient, ratio of the voltage transmitted to the incident voltage) measured at low temperature, when the crystal is in the superconducting state, and at $T = 40$ K, when the crystal is in the normal state. The experimental curves are fitted by $S_{21}(f) = S_{21}^{\max} \Big/ \sqrt{1 + Q_L^2(f/f_0 - f_0/f)^2}$, where f_0 is the resonance frequency and Q_L is the loaded quality factor. The unloaded quality factor, Q_0, is obtained as $Q_0 = Q_L/(1 - S_{21}^{\max})$. The way the presence of the K-Ba122 crystal affects the resonator parameters is shown in figures 1(b)–(d). The $1/Q_0(T)$ data are used for a definition of the critical temperature and of the width of the transition, as the FWHM of the derivative curve (see figure 1(e)).

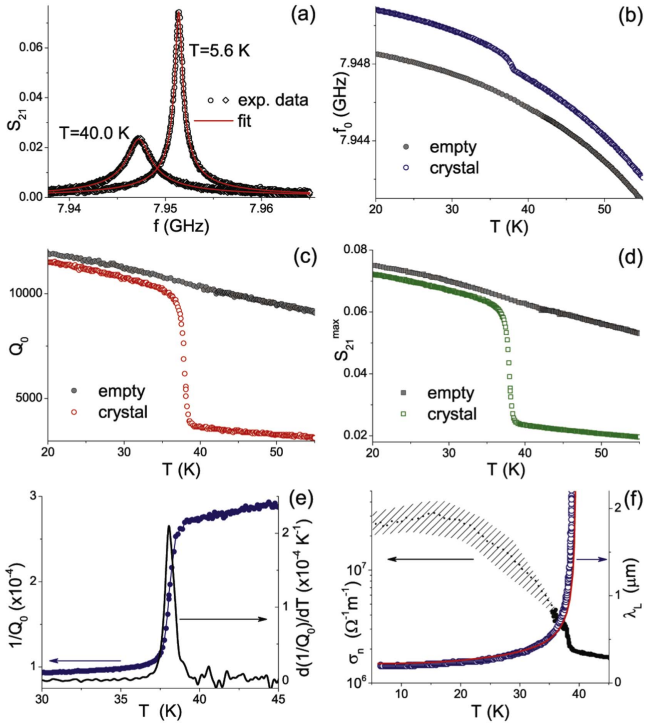

Figure 1. Survey of the microwave characterization technique. (a) S_{21} transmission coefficient as a function of frequency (resonance curve) of the YBCO resonator coupled to the K-Ba122 crystal under study, at two temperatures with the crystal in the superconducting state ($T = 5.6$ K) and in the normal state ($T = 40$ K). Data are fitted by the expression reported in the text. (b)–(d) Resonance frequency, unloaded quality factor and maximum transmission coefficient as a function of temperature for the empty resonator (grey symbols) and for the resonator coupled to the K-Ba122 crystal (blue, red and green open symbols). (e) Characterization of the K-Ba122 transition by the temperature derivative of the inverse of the quality factor. (f) London penetration depth (right) and quasiparticle conductivity (left) as a function of temperature, deduced from the experimental data shown above by the analysis reported in the text. Penetration depth experimental values are shown as open symbols, while the red line is the result of a calculation based on the solution of the Eliashberg equations within a three-band $s\pm$ model (detailed calculation and comparison with experimental data are reported in [25]). The shaded area in (f)-left represents the uncertainty in the absolute value of the quasiparticle conductivity, while the dotted line is the adjacent-averaging smoothing of the experimental points.

For what concerns data analysis, we started following the pioneering work by Hardy *et al* [26]. In brief, when a crystal is placed in the region of homogeneous magnetic field of the microwave resonator with the broad face parallel to the field, the perturbations relative to no sample in the cavity, in terms of resonance frequency fractional shift and quality factor modification are:

$$2\frac{\Delta f_0}{f_0} = \frac{V_s}{V_r}\left\{1 - \Re\mathfrak{e}\left[\frac{\tanh(kc)}{kc}\right]\right\}, \tag{1}$$

$$\Delta\left(\frac{1}{Q_0}\right) = \frac{V_s}{V_r}\Im\mathfrak{m}\left[\frac{\tanh(kc)}{kc}\right], \tag{2}$$

where k is the complex propagation constant, c is the crystal half-thickness, V_s is the volume of the sample, and V_r is the effective volume of the resonator. The geometrical factor

(V_s/V_r) cannot be calculated with the needed precision, especially for the open planar geometry of our resonator, but it can be determined in a self-consistent way from data above T_c, where the crystals show a metallic behavior. Moreover, the finite dimensions of the crystals are to be considered, resulting in the penetration of the field also from the lateral faces. The whole calibration procedure, taking into account also the size effects, is described in [25]. Once the geometrical factors are determined, equations (1) and (2) allow obtaining the real and imaginary parts of the propagation constant k in the superconducting state, and in turn the London penetration depth λ_L and the normal conductivity σ_n (see figure 1(f)), that are related to k by [27]: $k = \sqrt{\frac{1}{\lambda_L^2} + i\omega\mu_0\sigma_n}$. Finally, the surface impedance is calculated as [28]:

$$Z_s = R_s + iX_s = \frac{i\omega\mu_0\lambda_L}{\sqrt{1 + i\omega\mu_0\sigma_n\lambda_L^2}}. \quad (3)$$

2.3. Heavy-ion irradiations

250 MeV Au-ion irradiations were performed at room temperature at the Tandem-XTU facility of the LNL laboratories of the Italian National Institute for Nuclear Physics (INFN). The ion beam was parallel to the c-axis of the crystals and the ion flux was kept below $1.8 \times 10^8\,\mathrm{cm^{-2}\,s^{-1}}$, in order to avoid sample damage due to heating. Here we consider fluences up to $3.6 \times 10^{12}\,\mathrm{cm^{-2}}$. The crystals were selected with a thickness smaller than the longitudinal range of the ions into the material, to guarantee that defects are introduced without charge doping and implantation.

In the literature, Au-ions of comparable energy are reported to induce the formation of discontinuous tracks in IBS crystals [2]. The tracks are supposed to have a metallic core [9], instead of the insulating amorphous core of the tracks found in superconducting cuprates. In addition, other defects are produced, such as smaller cascades and point-like defects, also due to the effects of secondary electrons.

2.4. Damage simulation

In order to choose an adequate thickness of the samples to avoid ion implantation, Monte Carlo simulations were performed with both the SRIM [29] and PHITS [30] codes using the Kinchin–Pease approach. For 250 MeV Au-ions impinging on $Ba_{0.58}K_{0.42}Fe_2As_2$ the longitudinal range of the ions into the material was found to be about 14.5 μm. Figure 2 shows the electronic and the nuclear stopping power (the energy per unit path length released by a single ion through ionization or elastic coulombian scattering against the target nuclei, respectively) in the 10 μm of the crystal thickness, as calculated by the two codes. From the simulations one can also compute the overall damage in terms of d.p.a. (displacements per atom) and of the total energy released by ionization, E_i. The results obtained with the two codes are in reasonable agreement in the region of interest. An average

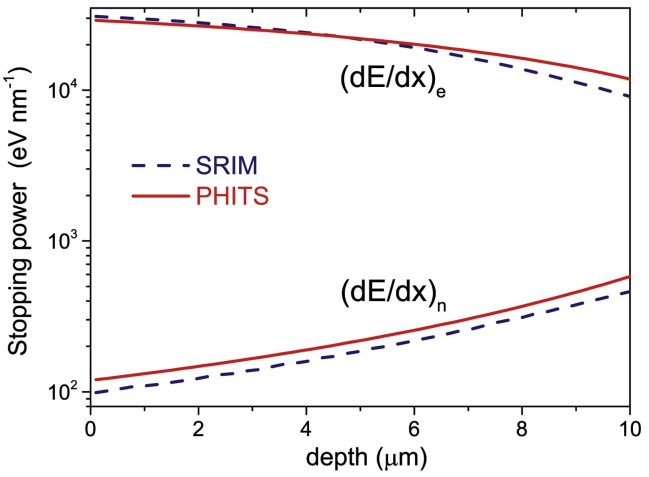

Figure 2. Energy per unit path length released by a 250 MeV Au ion in $Ba_{0.58}K_{0.42}Fe_2As_2$ by ionization (so-called electronic stopping power, $(dE/dx)_e$) and by elastic coulombian scattering against the target nuclei (nuclear stopping power, $(dE/dx)_n$). The stopping powers were calculated as a function of the depth into the material by means of the SRIM [29] and PHITS [30] codes.

over the thickness of the sample was performed yielding a mean d.p.a. value of $7.6 \times 10^{-16} \times \Phi$, and a total energy release by ionization of $2.1 \times 10^{11} \times \Phi\,\mathrm{eV\,cm^{-3}}$, if the fluence Φ is expressed in $\mathrm{cm^{-2}}$.

3. Results

3.1. Critical temperature and transition width

Data concerning critical temperature and transition width of some irradiated samples are summarized in figure 3. The critical temperature normalized to the value of the same crystal before irradiation is shown as a function of the d.p.a. (lower scale) and of the energy released by ionization (upper scale). The suppression of the critical temperature by disorder (i.e. by non-magnetic impurities) is weak, much weaker than in cuprates. This fact was initially used as an argument against the $s\pm$ wave model, but we have shown that, as a matter of fact, modifications of both λ_L and T_c by irradiation can be explained self-consistently within the $s\pm$ model, by considering a suitable description of the material with at least three bands [11]. The inset of figure 3 shows the broadening of the transition width due to irradiation, indicative of the level of induced disorder, as the FWHM of the derivative of $Q_0^{-1}(T)$ of the irradiated sample, substracted by the same quantity measured on the same crystal before irradiation. Data show a clear correlation with the critical temperature.

3.2. Surface impedance

Surface resistance and reactance are shown in figure 4 as a function of temperature, for a pristine crystal and for the same crystal after subsequent ion irradiations. The surface impedance conforms to the classical skin effect above the critical temperature, since $R_s = X_s$. A feature clearly emerges just

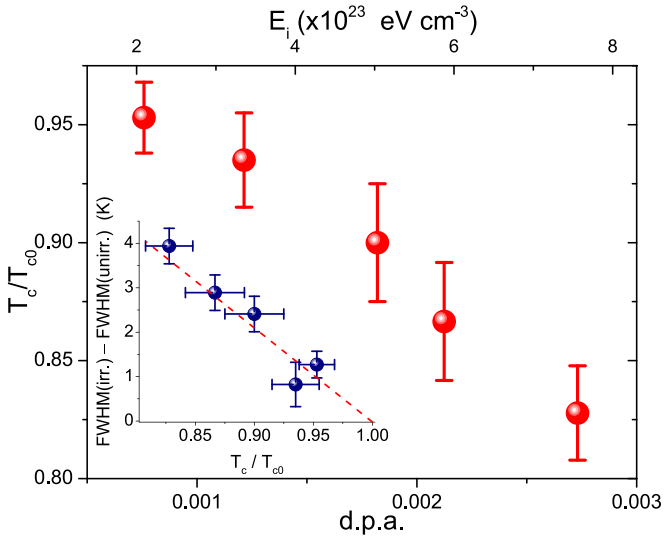

Figure 3. Critical temperature of the irradiated crystals, normalized to T_c of the corresponding crystals before irradiation, as a function of the displacements per atom (d.p.a., lower scale) and of the energy density released by ionization (E_i, upper scale), calculated on the base of SRIM [29] and PHITS [30] simulations. The inset shows the full width at half maximum of the $Q_0^{-1}(T)$ derivative, as an indication of the transition width increase after irradiation. Data are subtracted by the FWHM of the corresponding crystal before irradiation.

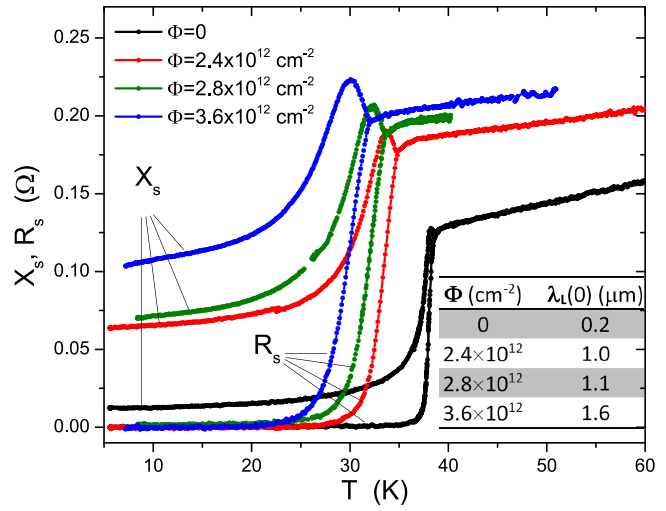

Figure 4. Real and imaginary parts of the surface impedance, $Z_s = R_s + iX_s$, as a function of temperature, for the same crystal before and after subsequent irradiations at fluence Φ. The table in the inset shows the values of the zero-temperature London penetration depth as a function of fluence.

below T_c, i.e. the presence of a peak in $X_s(T)$, which increases in size with irradiation. Such a peak can be explained within the two-fluid model: it arises because, on entering the superconducting state, the initial reduction in normal electrons is not immediately compensated, in terms of screening of the microwave field, by the increase of the superconducting current [31]. The X_s-peak temperature depends on $\omega\tau$, where τ is the carrier relaxation time and thus whether it appears or not depends both on the measurement conditions (ω) and on the material's properties (τ). Studying the $Z_s(T)$ curves within the two-fluid model gives the opportunity to gain information about electrodynamic parameters of the material.

3.3. Modified two-fluid model for the complex conductivity

In the standard two-fluid model, the surface impedance

$$Z_s = R_s + iX_s = \sqrt{i\mu_0\omega/(\sigma_1 - i\sigma_2)} \tag{4}$$

can be calculated by means of the following expression for the complex conductivity

$$\sigma_1 - i\sigma_2 = \frac{n_n e^2}{m^*}\frac{\tau}{1 + i\omega\tau} - \frac{i}{\mu_0\omega\lambda_L^2(T)}, \tag{5}$$

assuming that the conductivity of the normal fluid can be modeled by a Drude form, and $n_s(0) = n_s(T) + n_n(T)$, where n_s and n_n are the superfluid and quasiparticle densities, respectively, and considering the London relation $n_s(T) = m^*/(\mu_0 e^2\lambda_L^2(T))$.

Here we want to describe a general case, of arbitrary τ and when a fraction of the normal state electrons remains unpaired to the lowest temperatures, in order to include the effect of irradiation-induced disorder in a simple model. Thus, we assume that $n_s(0) + n_{RES} = n_s(T) + n_n(T)$, where n_{RES} is the density of the residual unpaired electrons. By defining $\epsilon = n_{RES}/n_s(0)$, the following expressions can be derived:

$$\sigma_1 = \left[\frac{1+\epsilon}{\mu_0\lambda_L^2(0)} - \frac{1}{\mu_0\lambda_L^2(T)}\right]\frac{\tau}{1+\omega^2\tau^2}, \tag{6}$$

$$\sigma_2 = \left[\frac{1+\epsilon}{\mu_0\lambda_L^2(0)} - \frac{1}{\mu_0\lambda_L^2(T)}\right]\frac{\omega\tau^2}{1+\omega^2\tau^2} + \frac{1}{\mu_0\omega\lambda_L^2(T)}, \tag{7}$$

where it is also assumed that the quasiparticle relaxation time, τ_{qp}, and the normal electron relaxation time, τ_n, are equal in the superconducting state.

There is evidence that the unirradiated material is clean and fully gapped [11] and therefore we assume $n_{RES} = 0$ in this case. This implies that, for the irradiated crystals, $\epsilon = \lambda_{L,irr}^2(0)/\lambda_{L,ni}^2(0) - 1$, where $\lambda_{L,ni}(0)$ and $\lambda_{L,irr}(0)$ are the zero-temperature London penetration depth values for the same crystal before and after irradiation, respectively (listed in the table reported in figure 4). Now, since $\lambda_L(T)$ is an output of the measurement and ω is given, equations (6)–(7) only depend on $\tau(T)$, and if a $\tau(T)$ dependence is assumed, the surface impedance can be calculated by equation (4).

4. Discussion

4.1. Fit of the $Z_s(T)$ curves

Figure 5 describes the analysis procedure in detail. In the upper panel (a) input data are shown, i.e. the experimental penetration depth $\lambda_L(T)$ and the relaxation time $\tau(T)$ that we assumed for the calculation. The $\tau(T)$ curve was changed until the experimental quasiparticle conductivity and the surface impedance were fitted by the curves calculated on the base of equations (4), (6) and (7), as reported (solid lines) in

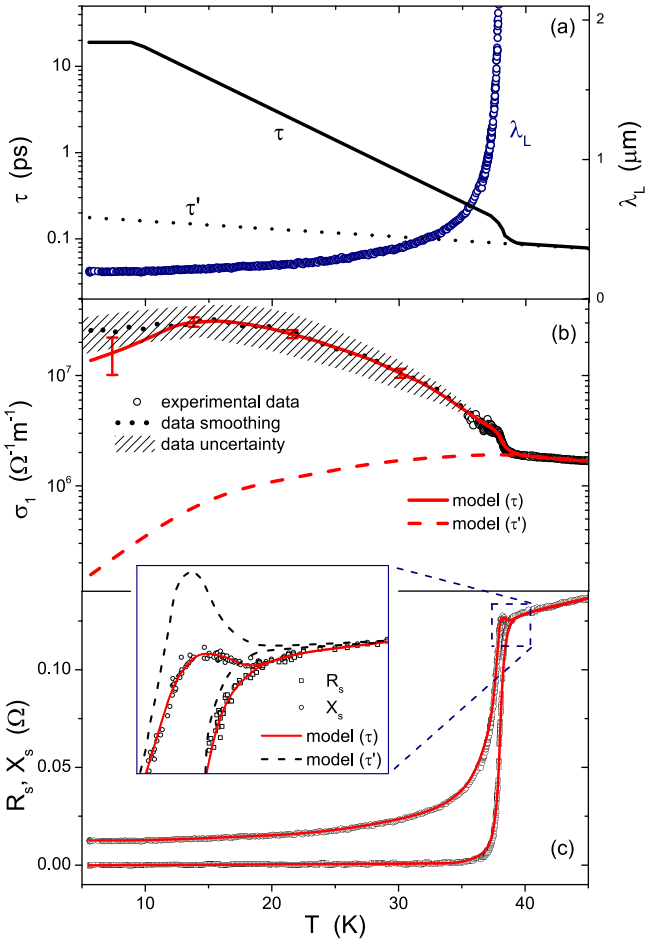

Figure 5. Description of the analysis procedure. (a) Input data: the experimental penetration depth $\lambda_L(T)$ and the relaxation time $\tau(T)$ that we assumed for the calculation for the unirradiated crystal. An alternative relaxation time is also indicated by $\tau'(T)$ (dotted line), for comparison (see below). (b) Real part of the experimental quasiparticle conductivity, compared to the curve calculated by equation (6) assuming $\lambda_L(T)$ and $\tau(T)$ shown in (a). The uncertainty for the experimental data is represented by the shaded area (the dotted line is a smoothing of data, as in figure 1(f)), while some representative error bars are shown for the calculated curve. The dashed line was calculated by assuming the alternative $\tau'(T)$ shown in (a) as a dotted line. The panel (c) shows a comparison between the experimental (symbols) and calculated (lines) real and imaginary parts of the impedance. Calculations were made based on equations (4), (6), (7), with $\lambda_L(T)$ and $\tau(T)$ shown in (a). The inset is a zoom of the curves close to the onset temperature, where a small peak in X_s emerges. The dashed lines were calculated by assuming $\tau'(T)$ as an input.

figures 5(b) and (c), respectively. As a first validation of the procedure, the value of $\tau(40\,\mathrm{K}) \approx 0.1$ ps for the unirradiated crystal shows nice agreement with previous results on $Ba_{1-x}K_xFe_2As_2$ [32].

As a comparison, a different assumption was also considered, i.e. a relaxation time that below T_c follows the same temperature dependence as above T_c, represented in figure 5(a) by a dotted line. This assumption, which was reported for copper-free perovskite superconductors [31], gives the correct temperature for the X_s-peak but overestimates its height and completely fails to fit the quasiparticle

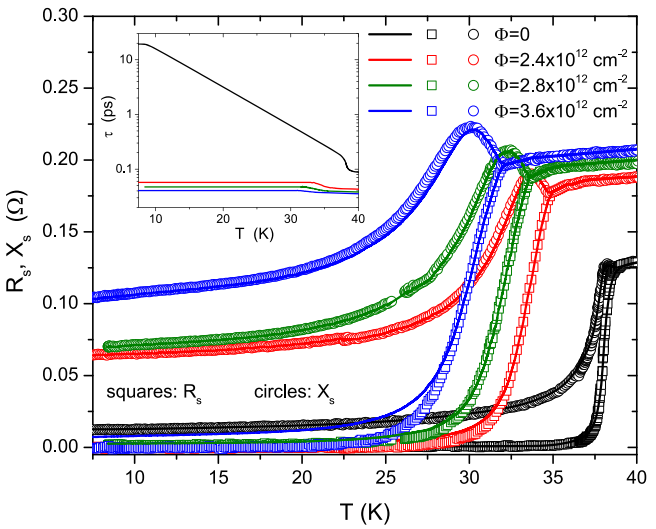

Figure 6. Real and imaginary parts of the surface impedance for the same crystal before and after irradiation at a fluence Φ. Experimental data (symbols, same data as in figure 4) are compared to calculations (solid lines) made within the modified two-fluid model described in the text. The calculated curves were obtained by $\tau(T)$ values reported in the inset.

conductivity (dashed lines in figures 5(b), (c)). In fact, it turns out that, in order to correctly fit the experimental data, a sudden increase of the relaxation time upon decreasing temperature across T_c is needed.

Figure 6 shows the real and imaginary parts of the surface impedance for the same crystal before and after subsequent irradiations. Experimental data were fitted by the procedure described above, with the relaxation time $\tau(T)$ values reported in the inset. It results that, while an increase of τ just below T_c is still needed, it becomes less and less significant as the irradiation-induced disorder is enhanced. The values of τ monotonically decrease after irradiation, both in the normal and in the superconducting states, down to about 0.04 ps. While τ at low temperatures for the unirradiated crystal increases by about two orders of magnitude with respect to its value at T_c, the relaxation times of the irradiated crystals appear quite flat.

Generally, the procedure seems to be successful for the unirradiated crystal and for the crystal irradiated at the lower doses, with reasonable fits of experimental $R_s(T)$ and $X_s(T)$ in the whole temperature range. However, at the highest dose significant deviations between data and calculation emerge (even if the X_S peak is still well reproduced), suggesting that the limits of validity of the present analysis have to be considered.

4.2. Limits of validity of the analysis

As noted above, after the irradiation at the highest fluence the τ temperature dependence resulting from the analysis appears quite flat. Moreover, to better fit low-temperature $R_s(T)$ experimental data, it seems that τ should even unphysically decrease at lower temperatures. In this case the risk exists to go beyond the limits of validity of the adopted analysis. In fact, the values of the effective quasiparticle density and the effective mass are determined by the Fermi sheet properties, depending on the relative contributions of the three sheets to

the electronic transport. We know from previous studies [11], that such properties are affected by disorder in a complex way, while in our analysis we implicitly considered the same total carrier density and the same effective mass for both unirradiated and irradiated samples. A calculation based on the actual multiband structure of the material and on its modification due to increased disorder—currently lacking in literature—is in progress, but is beyond the scope of this paper.

5. Conclusions

We have studied the electrodynamic response of $Ba_{1-x}K_xFe_2As_2$ single crystals at microwave frequencies, by means of a coplanar resonator technique, in samples where disorder was introduced by 250 MeV Au-ion irradiation. The surface impedance of the unirradiated and irradiated crystals is shown. It has been fitted across T_c within a modified two-fluid model, in order to investigate the influence of heavy-ion induced disorder on the material's electrodynamics, in particular on the quasiparticle relaxation time τ. To this aim, a finite quasiparticle fraction at $T = 0$ was assumed for the irradiated crystals. This simple model is able to describe the $Z_s(T)$ experimental data quite correctly and, in particular, to reproduce the $X_s(T)$ peak. The analysis gives τ (40 K) $\approx$ 0.1 ps for the unirradiated crystal, that is a value in good agreement with previous literature [32]. Irradiation is found to decrease τ, both in the normal and in the superconducting states, down to about 0.04 ps for the most irradiated crystal. Higher irradiation doses result in more flat $\tau(T)$ dependences and smaller differences across T_c. The low-temperature behavior of Z_s for the irradiated crystals, especially for the most irradiated one, raises the issue of the limits of application of the adopted model. They may stem from the fact that we considered the same total carrier density and the same effective mass for both unirradiated and irradiated samples, while they should depend on the relative contributions of the three Fermi sheets to the electronic transport, that are affected by disorder in a non-trivial way. Accounting for these effects is a challenging task, currently in progress.

Acknowledgments

The authors thank G A Ummarino for helpful discussions. This work was supported by MIUR-PRIN2012 Project No. 2012X3YFZ2. The irradiations were performed in the framework of the INFN-Politecnico di Torino M.E.S.H. Research Agreement.

ORCID iDs

G Ghigo https://orcid.org/0000-0003-3368-1319
D Torsello https://orcid.org/0000-0001-9551-1716
L Gozzelino https://orcid.org/0000-0002-9204-0792

References

[1] Karkin A E, Werner J, Behr G and Goshchitskii B N 2009 *Phys. Rev.* B **80** 174512
[2] Nakajima Y, Tsuchiya Y, Taen T, Tamegai T, Okayasu S and Sasase M 2009 *Phys. Rev.* B **80** 012510
[3] Tarantini C *et al* 2010 *Phys. Rev. Lett.* **104** 087002
[4] Nakajima Y, Taen T, Tsuchiya Y, Tamegai T, Kitamura H and Murakami T 2010 *Phys. Rev.* B **82** 220504(R)
[5] Tamegai T *et al* 2012 *Supercond. Sci. Technol.* **25** 084008
[6] Taen T, Yagyuda H, Nakajima Y, Tamegai T, Okayasu S, Kitamura H, Murakami T, Laviano F and Ghigo G 2013 *Phys. Supercond.* C **484** 62
[7] Taen T, Ohtake F, Akiyama H, Inoue H, Sun Y, Pyon S, Tamegai T and Kitamura H 2013 *Phys. Rev.* B **88** 224514
[8] Kihlstrom K J *et al* 2013 *Appl. Phys. Lett.* **103** 202601
[9] Massee F, Sprau P O, Wang Y-L, Davis J C S, Ghigo G, Gu G D and Kwok W-K 2015 *Sci. Adv.* **1** e1500033
[10] Moroni M, Gozzelino L, Ghigo G, Tanatar M A, Prozorov R, Canfield P C and Carretta P 2017 *Phys. Rev.* B **96** 094523
[11] Ghigo G, Ummarino G A, Gerbaldo R, Gozzelino L, Laviano F, Torsello D and Tamegai T 2017 *Sci. Rep.* **7** 13029
[12] Laviano F, Gerbaldo R, Ghigo G, Gozzelino L, Mikitik G P, Taen T and Tamegai T 2014 *Supercond. Sci. Technol.* **27** 044014
[13] Haberkorn N, Kim J, Maiorov B, Usov I, Chen G F, Yu W and Civale L 2014 *Supercond. Sci. Technol.* **27** 095004
[14] Ohtake F, Taen T, Pyon S, Tamegai T and Okayasu S 2014 *Phys. Proc.* **58** 122
[15] Cho K, Kończykowski M, Murphy J, Kim H, Tanatar M A, Straszheim W E, Shen B, Wen H H and Prozorov R 2014 *Phys. Rev.* B **90** 104514
[16] Mizukami Y *et al* 2014 *Nat. Commun.* **5** 5657
[17] Prozorov R, Kończykowski M, Tanatar M A, Thaler A, Bud'ko S L, Canfield P C, Mishra V and Hirschfeld P J 2014 *Phys. Rev.* X **4** 041032
[18] Mishev V, Nakajima M, Eisaki H and Eisterer M 2016 *Sci. Rep.* **6** 27783
[19] Ghigo G, Laviano F, Gerbaldo R and Gozzelino L 2012 *Supercond. Sci. Technol.* **25** 115007
[20] Ghigo G, Gerbaldo R, Gozzelino L, Laviano F and Tamegai T 2016 *IEEE Trans. Appl. Supercond.* **26** 7300104
[21] Ghigo G, Andreone D, Botta D, Chiodoni A, Gerbaldo R, Gozzelino L, Laviano F, Minetti B and Mezzetti E 2005 *Supercond. Sci. Technol.* **18** 193
[22] Ghigo G, Gerbaldo R, Gozzelino L, Laviano F, Lopardo G, Monticone E, Portesi C and Mezzetti E 2009 *Appl. Phys. Lett.* **94** 052505
[23] Ghigo G, Botta D, Chiodoni A, Gozzelino L, Gerbaldo R, Laviano F, Mezzetti E, Monticone E and Portesi C 2005 *Phys. Rev.* B **71** 214522
[24] Ghigo G, Laviano F, Gozzelino L, Gerbaldo R, Mezzetti E, Monticone E and Portesi C 2007 *J. Appl. Phys.* **102** 113901
[25] Ghigo G, Ummarino G A, Gozzelino L and Tamegai T 2017 *Phys. Rev.* B **96** 014501
[26] Hardy W N, Bonn D A, Morgan D C, Liang R and Zhang K 1993 *Phys. Rev. Lett.* **70** 3999
[27] Vendik I B 2000 *Supercond. Sci. Technol.* **13** 974
[28] Vendik I B and Vendik O G 1997 *High Temperature Superconductor Devices for Microwave Signal Processing—Part II* (St. Petersburg: Sclanden)
[29] Ziegler J F, Ziegler M D and Biersack J P 2010 *Nucl. Instrum. Methods Phys. Res.* B **268** 1818
[30] Sato T *et al* 2013 *J. Nucl. Sci. Technol.* **50** 913
[31] Ormeno R J, Hein M A, Barraclough T L, Sibley A, Gough C E, Mao Z Q, Nishizaki S and Maeno Y 2006 *Phys. Rev.* B **74** 092504
[32] Hashimoto K *et al* 2009 *Phys. Rev. Lett.* **102** 207001